RESEARCH ARTICLE
doi: 10.2306/scienceasia1513-1874.2020.023

ScienceAsia 46 (2020): **169–177**

Fabrication of PVC/MWNTs-g-C_{16} composites with high solar-thermal conversion performance for anti-icing and deicing

Xiaoning Shen[a], Lihuan Yuan[a], Zhen Wei[a], Yujun Qin[b,*], Yapei Wang[b], Zhi-Xin Guo[b,*], Lili Geng[a]

[a] Department of Applied Chemistry, College of Science, Hebei North University, Zhangjiakou, China
[b] Department of Chemistry, Renmin University of China, Beijing 100872 China

*Corresponding authors, e-mail: yjqin@ruc.edu.cn, gzhixin@ruc.edu.cn

Received 14 Jan 2020
Accepted 17 Mar 2020

ABSTRACT: In this study, an easy method is presented to prepare a polymer based multi-walled carbon nanotube (MWNT) composite. First, MWNTs grafted to n-hexadecyl bromide (MWNTs-g-C_{16}) were prepared using an esterification reaction of carboxylate salt on the MWNTs' surface and a bromine group consisting of n-hexadecyl bromide in the presence of a phase-transfer reagent in water. Subsequently, a composite material of PVC/MWNTs-g-C_{16} was prepared by melt blending with a series of dissolvable MWNTs-g-C_{16} aided by heat stabilizers and lubricants. Thermogravimetric analysis of the MWNTs-g-C_{16} showed a weight percentage of attached alkyl chains as high as 35.77 wt%, and a TEM image proved that the soluble MWNTs-g-C_{16} were well dispersed randomly in a matrix of polyvinyl chloride (PVC). Solar-thermal conversion performances of the PVC/MWNTs-g-C_{16} composites were studied, and the composites exhibited excellent light absorption properties. This property is attributed to the optical absorption characteristics of MWNTs. The PVC/MWNTs-g-C_{16} composite material exhibits excellent mechanical properties, and could be used as solar collectors or as solar anti-icing and deicing materials.

KEYWORDS: polymer based carbon nanotubes composite, polyvinyl chloride, solar-thermal conversion

INTRODUCTION

Very rapid progress has been made in the research of polymer based carbon nanotube (CNT) composites. The two methods of preparation of polymer based CNT composites include surface modified CNTs blended with a matrix polymer using solvent blending or melt blending, and the other method includes chemical grafting. Polymer or hyper-branched polymer is blended or grafted onto the surface of a CNT using direct introduction, surface initiation polymerization, step growth, or a combination of clicking chemistry. Long alkyl chains can be grafted on the surface of CNTs using a chemical grafting modification that can effectively reduce the space hindrance effect of CNTs and the intertwining between CNTs. This method [1] can effectively improve the dispersion of CNTs in the solvent or the polymer matrix, and the longer the alkyl chain, the better the solubility and dispersion. Due to the remarkable electrical, thermal, optical, and mechanical properties, CNTs have become an ideal material for improving these properties of polymer composites. For example, the high elastic modulus and high strength of the CNTs are 10–100 times higher than the highest strength steel [2]. CNTs also have unique electrical properties and current carrying capacities [3, 4]. In addition, they have unique solar-thermal properties and can efficiently convert light into heat [5–7].

Polymer based CNT composites have many potential applications, such as applications in super materials, flexible displays, electronic paper for bulletproof vests, solar energy collectors [8, 9], infrared thermal detectors [10], efficient infrared heaters [11] and electric heating material for deicing [12, 13]. Ice accretion on facilities has become a serious economic and safety issue [14–17] and the combination of a hydrophobic surface with a photothermal effect is an effective method to achieve the combination of active and passive deicing. Some nano-particles (such as CNTs) can perform this function since they can absorb solar radiation for heating [18–21]. There are two theories that explain the absorption characteristics and photothermal conversion of CNTs. One theory claims that the above characteristics come from the vertically aligned structure of CNTs [6]. The other states that

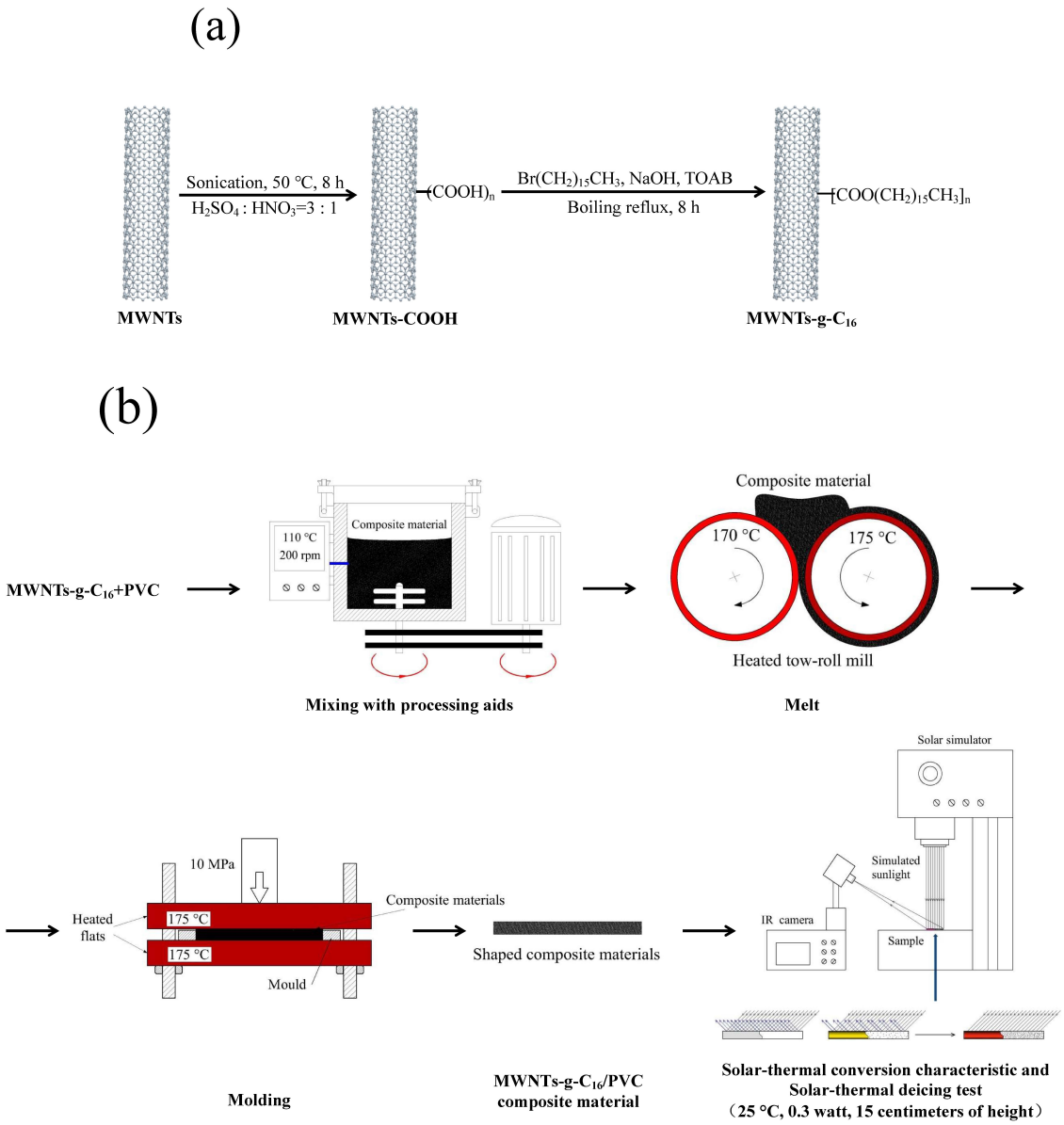

Fig. 1 Schematic diagram for (a) the synthesis of MWNTs-g-C_{16}, (b) the preparation and solar-thermal conversion characteristic test of PVC/MWNTs-g-C_{16} composite materials.

they are caused by the unique electronic structure of CNTs [22, 23]. This photo-thermal performance has wide application prospects, such as for drug delivery systems and cancer therapies in the field of biomedicine [24], for remote thermal reactions in the field of energy science [25, 26], and for phase transitions of polymer gel hybrids in the field of materials science [27, 28].

In this work, a solar-thermal anti-icing and de-icing composite consisting of PVC/MWNTs-g-C_{16} is proposed for the first time. Fig. 1 depicts graphically the synthesis route of MWNTs-g-C_{16}, the preparation route of the target product PVC/MWNTs-g-C_{16} and solar-thermal conversion characteristic test. MWNT surface was modified with carboxylic-acid groups through acid treatment and then the functional MWNT reacted with n-hexadecyl bromide to yield MWNTs-g-C_{16} with long aliphatic chains with ester linkages. The whole reaction was carried out in water for several hours, which is a

simpler and more efficient method [1] based on the phase-transfer esterification between carboxylate salts and halohydrocarbon. Finally, a novel composite material of PVC/MWNTs-g-C_{16} with a random arrangement of MWNTs was attained by melting and molding the MWNTs-g-C_{16} and PVC aided by heat stabilizers and lubricants. In addition, the solar-thermal deicing and mechanical properties were characterized.

MATERIALS AND METHODS

Materials

Tetra-n-octylammonium bromide and n-hexadecyl bromide used in this study were analytical grade, and purchased from the J&K Scientific Technology Co., Ltd. (China). Polyvinyl chloride (the degree of polymerization was 1000, universal grade) was supplied by the Xinjiang Zhongtai Chemical (Group) Co., Ltd. All other solvents and reagents were chemical pure.

Preparation of PVC/MWNTs-g-C_{16}

The MWNTs used in this work were prepared using the chemical vapour deposition method developed by the Suzhou TANFENG Graphene Tech Co., Ltd, China. The MWNTs were purified and converted into carboxylic MWNTs (MWNTs-COOH) by sonication in nitric acid-sulfuric acid (Fig. 1). The resultant solid was washed thoroughly with deionized water, sonicated in NaOH solution to convert carboxylic groups to sodium-salt form. Then tetra-n-octylammonium bromide and n-hexadecyl bromide were added into the suspension before refluxing with vigorous stirring. Finally, the suspension became clear with black precipitate. The precipitate was collected, washed with ethyl alcohol, and then extracted with tetrahydrofuran (THF) to remove all unwanted impurities. The black solid of MWNTs-g-C_{16} was collected and dried in a vacuum. Samples 1–5 were prepared by mixing different parts of MWNTs-g-C_{16} (0, 0.01, 0.05, 0.10, 0.25) with polyvinyl chloride (PVC) resin and processing aids (100 parts of PVC, 2.0 parts of heat stabilizer, 0.8 part of calcium stearate, and 0.8 part of stearic acid) in a stainless steel high-speed mixer at 105 °C, a grey powder of PVC/MWNTs-g-C_{16} due to the embedding of the MWNTs in the PVC was obtained. Then the mixture was melted and mixed on a laboratory two-roll mill at 175 °C, MWNTs were better dispersed in the matrix and the final PVC/MWNTs-g-C_{16} composite material test plates obtained from molding turned into black.

Characterization of PVC/MWNTs-g-C_{16}

Thermogravimetric analysis (TGA) experiments were performed to analyze the alkyl-modified MWNTs. TGA was performed using a TGA Q50 instrument (TA Instruments, Inc., New Castle, DE) at a scanning rate of 10 °C/min from room temperature up to 800 °C under N_2 flow. Scanning electron microscopy (SEM) images were recorded using a Hitachi SU8010 field-emission microscope. High vacuum conditions were applied, and a secondary electron detector was used for image acquisition. Transmission electron microscopy (TEM) images were obtained using a JEOL-3010 ultra-high-resolution transmission electron microscope. A typical specimen used for TEM analysis was a 50 nm frozen section of a sample. Tensile strength and bending strength tests were performed using an RGT-10A electronic tensile tester with a computer control system according to the china standards of GB/T1040.2-2006 and GB/T9341-2008. The notched impact strength test was carried out on an XCJ-40 Charpy impact tester according to the china standards of GB/T 1043.1/1eA^b-2008. The dumbbell specimen used for tensile strength testing had dimensions of 150 mm long with a cross-section of 4×10 mm^2, and the tests were conducted at an extension rate of 20 mm/min. The size of the samples for the bending strength test were $80 \times 10 \times 4$ mm^3, and the tests were conducted at a rate of 20 mm/min. The size of the samples for the notched impact strength tests were $80 \times 10 \times 4$ mm^3, and the notch depth was equal to 1/5 of the thickness of the sample. Tests were conducted at 23 °C and 50% relative humidity.

The solar-thermal conversion efficiency and thermal conductivity of these materials are very important for their use as solar-thermal energy harvesters. The experimental results of solar-thermal conversion are shown in Fig. 1. The sample temperature increased as recorded every 5 s by a high-resolution infrared camera. After 2 min, the sunlight source was turned off and the sample temperature was recorded for a further 2 min. The solar-thermal conversion properties of PVC/MWNTs-g-C_{16} composite samples with different amounts of MWNTs-g-C_{16} were characterized using the above experimental methods, and the relative curves between temperatures of samples and test times were obtained.

To investigate the effectiveness of the application of the PVC/MWNTs-g-C_{16} composite materials on deicing, an experiment was conducted indoors

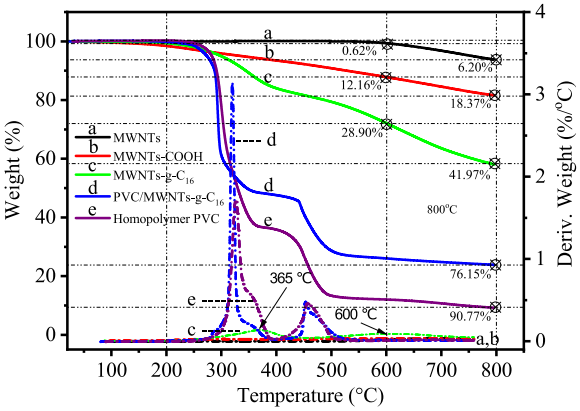

Fig. 2 Thermogravimetric (solid lines) and derivative (dashed lines) curves of MWNTs, MWNTs-COOH, MWNTs-g-C_{16}, PVC/MWNTs-g-C_{16} and homopolymer PVC. The content of MWNTs-g-C_{16} is 0.25%.

at 26 °C under windless conditions. The height of the icicle on the sample surface was 20 mm (2 g). The deicing times and temperatures were recorded under a simulated solar light condition (0.3 watt) and no light condition on both Si and PVC/MWNTs-g-C_{16} composite substrates, as shown in Fig. 1.

RESULTS AND DISCUSSION

Thermogravimetric analysis (TGA)

As shown in Fig. 2, the small mass loss (0.62%) of pristine MWNTs was not obvious when the temperature reached 600 °C, and the final mass loss upto 800 °C was ∼6.2%, corresponding to the thermal oxidation of the remaining disordered carbon and residual impurities during preparation [29]. Two temperature regions of mass loss existed for the MWNTs-COOH. One mass loss occurred at 12.16% between 150 °C and 600 °C and was attributed to the removal of attached carboxyl groups [30]. The other occurred at 6.21% between 600 °C and 800 °C, belonging to the decomposition of amorphous carbon, similar to MWNTs. MWNTs-g-C_{16} also displayed two temperature regions of mass loss. The one between 200 °C and 600 °C was attributed to the decomposition of alkyl groups [31]. The other between 600 °C and 800 °C was attributed to the simultaneous decomposition of amorphous carbon. The mass loss was 28.90% up to 600 °C, corresponding to the removal of attached alkyl groups, which could be used to estimate the mass percentage of alkyl groups that were attached to the tubes. The nanotube content of the MWNTs-g-C_{16} was 71.10%.

The TGA curves of the homopolymer PVC and PVC/MWNTs-g-C_{16} had two temperature regions of mass loss. The first weight loss stage of 250–350 °C was attributed to the rapid removal of HCl initiated by the production of chlorine radicals, the second weight loss stage of 400–800 °C was attributed to the structural rearrangements, such as isomerization and aromatization. The total mass loss was 76.15% up to 800 °C of PVC/MWNTs-g-C_{16}, 14.62% less than 90.77% of homopolymer PVC. This was due to the presence of processing aids and MWNTs-g-C_{16} in the PVC/MWNTs-g-C_{16} that was not amenable to decomposition.

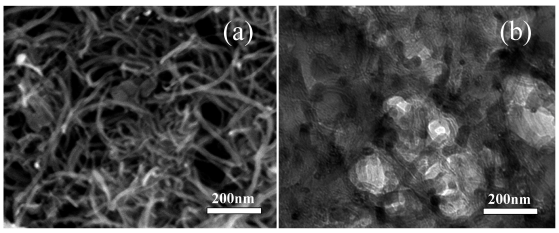

Fig. 3 (a) SEM image of MWNTs-g-C_{16} and (b) TEM image of PVC/MWNTs-g-C_{16} composite materials.

Electron microscopy

The SEM and TEM images provide direct proof of the existence and the shape of carbon nanotubes in the samples. In Fig. 3, the typical SEM image of the MWNTs-g-C_{16} and the TEM image of the PVC/MWNTs-g-C_{16} composite material are shown. In both the SEM and TEM images of the samples, the average length and diameter of the nanotube was 2 μm and 20 nm, respectively. The two images show that the tube wall structure was consistently complete. The dispersion morphology of the MWNTs-g-C_{16} in the matrix PVC is visible in the TEM image. The MWNTs-g-C_{16} was well dispersed with a random three-dimensional network-like arrangement. TEM image of the PVC/MWNTs-g-C_{16} composite material shows that MWNTs have the same state of morphology as that of the MWNT-g-PVC, another kind of solar-thermal material prepared by this research group [32]. As Ornatska [33] concluded, the functionalization of CNTs was an important mean to improve the solubility and dispersion of CNTs in solvents and polymer matrix.

Mechanical properties

Tensile strength and elongation at breaks

The influence of the MWNTs-g-C_{16} content on the tensile strength and the elongation at breaks is

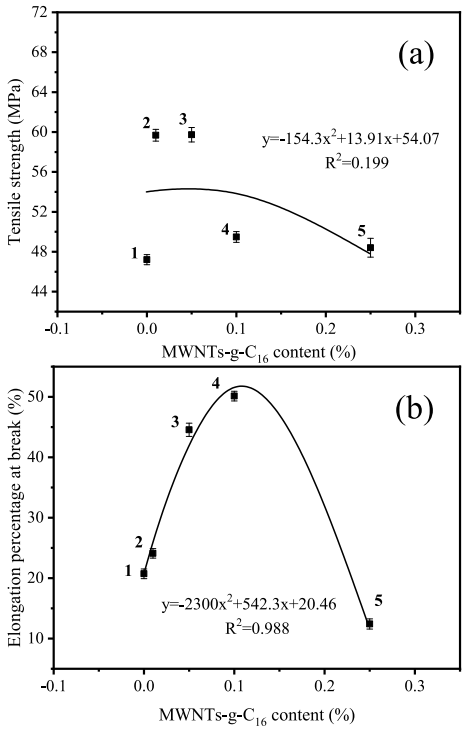

Fig. 4 Influence of MWNTs-g-C_{16} content on (a) tensile strength and (b) elongation at breaks in the materials. Samples 1 to 5 are as described in Fig. 7.

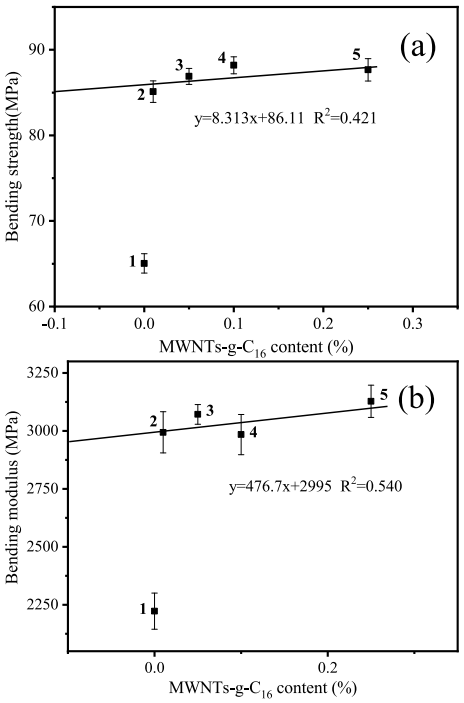

Fig. 5 Influence of MWNTs-g-C_{16} content on (a) bending strength and (b) bending modulus of the materials. Samples 1 to 5 are as described in Fig. 7.

shown in Fig. 4. The statistical analysis showed that the curve between elongation at breaks or the tensile strength and MWNTs-g-C_{16} content was similar to parabola, though the tensile strength curve showed a lower correlation than the curve of the elongation at breaks. According to the fitting curves, for the composites with MWNTs-g-C_{16} content in the range of 0–0.25%, the values of tensile strength and elongation at breaks of each sample were more or less reliable judging from the standard deviations shown in the graphs. The tensile strength of the materials increased with increasing MWNTs-g-C_{16} content, and the elongation at the break was markedly increased when the content of the MWNTs-g-C_{16} was less than 0.1%. There was a maximum tensile strength in the relationship curve, similar to the elongation at the break. The tensile strength of the composites was enhanced to approximately 130% of the tensile strength of pure PVC, while its elongation at the break was approximately 2.5 times that of pure PVC. However, the tensile strength and elongation at the break of the composites decreased sharply by increasing the MWNTs-g-C_{16} content to more than 0.1%. The results are related to the agglomerating structure of the MWNTs-g-C_{16}. The agglomeration of MWNTs-g-C_{16} could reduce the mechanical properties of the composites, causing a decline in strength when the MWNTs-g-C_{16} was used as reinforcing agent. After modification, a large number of long alkyl chain groups were present on the surface of MWNTs. This not only effectively prevents MWNT aggregation, but also improves the dispersion when the content of modified MWNTs falls below 0.1% in the PVC matrix. However, the MWNTs-g-C_{16} can partially agglomerate with an increase of content in the matrix. Our results about mechanical properties of polymer nanocomposites agree with those summarized by Miyagawa [34], and Tjong [35]. So CNTs are ideal reinforcement for polymers [36].

Bending strength and bending modulus

The bending strength and bending modulus of the composites with varying MWNTs-g-C_{16} contents in an otherwise fixed condition are shown in Fig. 5. The bending strength and bending modulus of the materials were obviously increased with an increase in the MWNTs-g-C_{16} content. The bending strength and bending modulus of the composites were en-

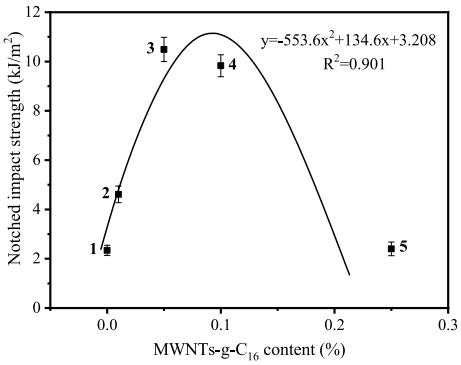

Fig. 6 Influence of MWNTs-g-C_{16} content on the notched impact strength of materials. Samples 1 to 5 are as described in Fig. 7.

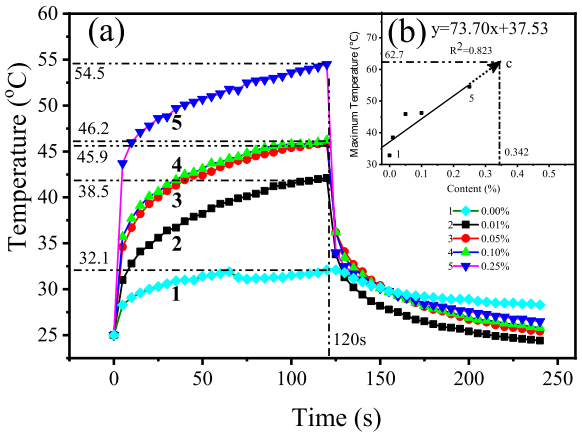

Fig. 7 Solar-thermal conversion performance of homopolymer PVC (sample 1) and MWNTs-g-C_{16} composite material film with different parts (samples 2–5). The inset shows the straight line (solid line) fitted by maximum temperatures and its extended part (dotted line with arrow.)

hanced to approximately 140% of that of pure PVC. The bending performances of the composites are mainly related to the dispersion state and dispersion capacity of the MWNTs-g-C_{16} in the matrix of the PVC. The statistical analysis showed that the relationship between bending strength or bending modulus and MWNTs-g-C_{16} content was close to linear. According to the fitting lines for the composites with MWNTs-g-C_{16} content in the range of 0–0.25%, the values of bending strength and bending modulus of each sample were more or less reliable judging from the standard deviations shown in the plots. The compatibility of MWNTs with PVC matrix was increased after alkylation, resulting in a good interface interaction between the two phases, so the MWNTs-g-C_{16} play a good role in the reinforcement of PVC matrix. When MWNTs-g-C_{16} content was less than 0.25%, it effectively dispersed in the matrix of the PVC, and the reinforced PVC matrix was similar to the fiber. These results about mechanical properties agree with those found experimentally by Yang [37] and Shi [38] who observed increases in moduli and strength with polymer-grafted carbon-nanotubes. The excellent mechanical properties provide the basis for the application of PVC/MWNTs-g-C_{16} composites.

Impact strength

Fig. 6 shows the impact strength results of the materials with varying MWNTs-g-C_{16} content. At less than 0.1% of MWNTs-g-C_{16}, the notched impact strength of the materials significantly increased when the nanocomposites increased. While at more than 0.1%, the impact strength of the sample was obviously decreased. The statistical analysis showed that the curve between impact strength and MWNTs-g-C_{16} content was similar to parabola with a high correlation. According to the fitting curve for the composites with MWNTs-g-C_{16} content in the range of 0–0.25%, the values of impact strength of each sample were more or less reliable judging from the standard deviations shown in the graphs. The maximum notched impact strength of the composites was nearly five times higher than that of PVC. The toughening effect of the MWNTs-g-C_{16} is chiefly attributed to the content and dispersion of MWNTs-g-C_{16} in the PVC matrix, this agrees well with the carbon fiber reinforcement summarized by Coleman [39] and Blake [40]. When the amount of carbon reaches a certain level, the agglomeration structure of MWNTs-g-C_{16} causes the decrease in the toughening performance of composites [41]. Although the modification of a large number of long alkyl chains can effectively prevent the agglomeration of MWNTs and improve the dispersion in the PVC matrix, this effect is limited to low-content conditions.

Solar-thermal conversion characteristics

As shown in Fig. 7a. The temperature of all the samples gradually rose with continuous illumination, and gradually dropped when the solar light source was turned off. However, the solar-thermal conversion efficiency and thermal conductivity of each sample with different amounts of MWNTs-g-C_{16} were significantly different from each other.

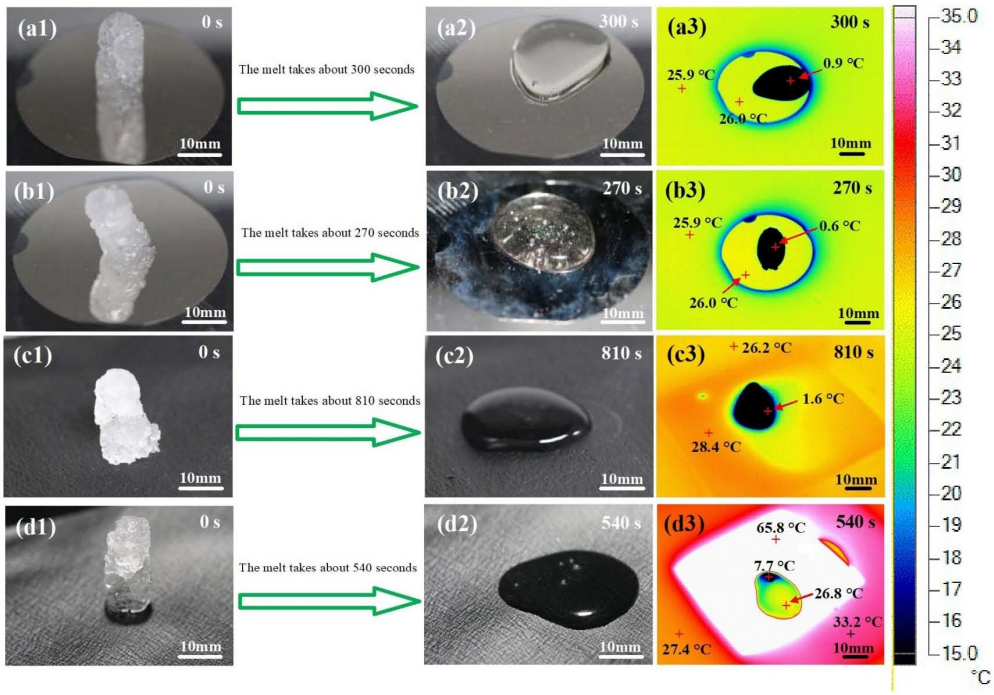

Fig. 8 Deicing photo (one picture per 30 s) and infrared thermal image after the ice completely dissolved: (a,b) simulated solar light (0.3 watt) and no light conditions on a silicon substrate; (c,d) simulated solar light and no light conditions on a PVC/MWNTs-g-C_{16} composite substrate. The content of MWNTs-g-C_{16} is 0.25%.

Homopolymer PVC did not easily absorb solar lights and effectively converts them into heat energy, therefore, the maximum temperature of sample 1 was only 32.1 °C after 2 min of illumination. The solar-thermal conversion capability of the composites increased with an increase in MWNTs-g-C_{16} content, and the highest efficiency was found in sample 5 with a 2.5% content and a maximum temperature of 54.5 °C, which was 22.4 °C higher than that of the homopolymer PVC. The PVC/MWNTs-g-C_{16} composites exhibited an excellent solar-thermal conversion performance, although the MWNTs in the PVC/MWNTs-g-C_{16} composites exhibited no alignment, and the optical absorption performances were comparable with that of the vertical CNTs array [42]. The faster the sample cools, the better the thermal conductivity after the light source is closed. So the thermal conductivity efficiency for sample 2 with 0.01% content was the highest, while the homopolymer PVC had the lowest thermal conductivity. According to Fig. 7b, a linear relationship between the maximum temperature and MWNTs-g-C_{16} content was obtained with a good correlation. The maximum temperature of the samples increased linearly with an increase in the MWNTs-g-C_{16} content. The slope of this straight line was far less than that of the MWNT-g-PVC(229.97) line, another kind of solar-thermal material prepared by our research group [32]. Although the solar-thermal conversion efficiency of the PVC/MWNTs-g-C_{16} prepared using melt bending was lower than that of the MWNT-g-PVC composites prepared using chemical grafting, this method is simple and feasible. In addition, it is easier to achieve large-scale preparation of the PVC/MWNTs-g-C_{16} composite material. An equivalent solar-thermal conversion effect of the MWNT-g-PVC composites was obtained by increasing the content of MWNTs-g-C_{16} during blending.

Solar-thermal deicing properties

As shown in Fig. 8, the deicing time is 540 seconds under simulated solar light for the PVC/MWNTs-g-C_{16} composite substrate which is 270 seconds shorter than that under no light condition. This is a one-third reduction in deicing time.

The two infrared thermal images of the PVC/MWNTs-g-C_{16} substrates were completely different from each other and the image of the Si substrate. In the absence of simulated solar light for

deicing, the PVC/MWNTs-g-C_{16} substrate absorbed the light in the laboratory and converted it into heat, so the substrate temperature (28.4 °C) was higher than the workbench temperature (26.2 °C). This indicated that the PVC/MWNTs-g-C_{16} composite absorbed various light wavelengths. In contrast, as shown in the infrared thermal image of PVC/MWNTs-g-C_{16} substrate under simulated solar light, the temperature of the PVC/MWNTs-g-C_{16} substrate was 65.8 °C. This was approximately 40 °C higher than the room temperature and the workbench temperature (27.4 °C). There was a very obvious temperature gradient between the PVC/MWNTs-g-C_{16} substrate and the workbench, also caused by heat conduction. The experimental results show that the PVC/MWNTs-g-C_{16} composite substrate effectively absorbed the simulated solar light and transformed it into heat, which increased the substrate's temperature and increased the speed of melting ice.

CONCLUSION

In summary, a series of PVC/MWNT-g-C_{16} composites with different photo-thermal conversion capabilities were obtained by phase-transfer esterification and melt blending. The incorporation of MWNTs into PVC exhibited a randomly arranged structure. The modification of a large number of long alkyl chains could improve the dispersion of MWNTs in the PVC matrix, so the modified MWNTs had a good effect on the reinforcement and toughening of PVC matrix in low-content conditions. The composites could trap solar radiation efficiently and convert it to heat due to the intrinsic properties of CNTs, presenting excellent optical absorption and solar-thermal conversion performance. Moreover, the method of melt blending was relatively simple and practicable, and the composites prepared had significant film-forming ability for the post-processing techniques into films, sheets, and plates with desired shapes and sizes. This composite material is expected to be used as an anti-icing and deicing coating materials, or applied in the field of heat-conduction devices and solar-thermal energy harvesters, even in biomedical fields such as drug delivery systems and cancer treatment.

Acknowledgements: This work was supported by the National Natural Science Foundation of China (Grant Nos. 21422407, 21473250, and 21773305), the Fundamental Research Funds for the Central Universities, and the Research Funds of Renmin University of China (Grant Nos. 15XNLQ04 and 16XNLQ04).

REFERENCES

1. Qin YJ, Shi JH, Wu W, Li XL, Guo ZX, Zhu DB (2003) Concise route to functionalized carbon nanotubes. *J Phys Chem B* **107**, 12899–12901.
2. Yu MF, Files BS, Arepalli S, Ruoff RS (2000) Tensile loading of ropes of single wall carbon nanotubes and their mechanical properties. *Phys Rev Lett* **84**, 5552–5555.
3. Collins PG, Avouris P (2000) Nanotubes for electronics. *Sci Am* **283**, 62–69.
4. Frank S, Poncharal P, Wang ZL, de Heer WA (1998) Carbon nanotube quantum resistors. *Science* **280**, 1744–1746.
5. Du XS, Xu JN, Deng S, Du Z, Cheng X, Wang HB (2019) Amino-functionalized single-walled carbon nanotubes-integrated polyurethane phase change composites with superior photothermal conversion efficiency and thermal conductivity. *ACS Sustain Chem Eng* **7**, 17682–17690.
6. Mizuno K, Ishii J, Kishida H, Hayamizu Y, Yasuda S, Futaba DN, Yumura M, Hata K, et al (2009) A black body absorber from vertically aligned single-walled carbon nanotubes. *Proc Natl Acad Sci USA* **106**, 6044–6047.
7. Gokhale VJ, Shenderova OA, McGuire GE, Rais-Zadeh M (2014) Infrared absorption properties of carbon nanotube/nanodiamond based thin film coatings. *J Microelectromech Syst* **23**, 191–197.
8. Shashikala AR, Sharma AK, Bhandari DR (2007) Solar selective black nickel-cobalt coatings on aluminum alloys. *Sol Energy Mater Sol Cells* **91**, 629–635.
9. Li XK, Chen WJ, Zou CJ (2020) An experimental study on beta-cyclodextrin modified carbon nanotubes nanofluids for the direct absorption solar collector (DASC): Specific heat capacity and photothermal conversion performance. *Sol Energy Mater Sol Cells* **204**, ID 110240.
10. Theocharous E, Lehman J (2011) The evaluation of a pyroelectric detector with a sprayed carbon multiwall nanotube black coating in the infrared. *Infrared Phys Techn* **54**, 34–38.
11. Granqvist CG (1981) Radiative heating and cooling with spectrally selective surfaces. *Appl Opt* **20**, 2606–2615.
12. Chu HT, Zhang ZC, Liu YJ, Leng JS (2014) Self-heating fiber reinforced polymer composite using meso/macropore carbon nanotube paper and its application in deicing. *Carbon* **66**, 154–163.
13. Wu JJ, Li HQ, Lai XJ, Chen ZH, Zeng XR (2019) Superhydrophobic polydimethylsiloxane multiwalled carbon nanotubes membrane for effective water-in-Ooil emulsions separation and quick deicing. *Ind Eng Chem Res* **58**, 8791–8799.
14. Marwitz J, Politovich M, Bernstein B, Ralph F, Neiman P, Ashenden R, Bresch J (1997) Meteorolog-

ical conditions associated with the ATR72 aircraft accident near Roselawn, Indiana on 31 October 1994. *Bull Am Meteorol Soc* **78**, 41–53.
15. Mishchenko L, Hatton B, Bahadur V, Taylor JA, Krupenkin T, Aizenberg J (2010) Design of ice-free nanostructured surfaces based on repulsion of impacting water droplets. *ACS Nano* **4**, 7699–7707.
16. Laforte JL, Allaire MA, Laflamme J (1998) State-of-the-art on power line de-icing. *Atmos Res* **46**, 143–158.
17. Parent OA (2011) Anti-icing and de-icing techniques for wind turbines: Critical review. *Cold Reg Sci Technol* **65**, 88–96.
18. Nardecchia S, Carriazo D, Ferrer ML, Gutierrez MC, Monte FD (2013) Three dimensional macroporous architectures and aerogels built of carbon nanotubes and/or graphene: synthesis and applications. *Chem Soc Rev* **42**, 794–830.
19. Badenhorst H (2019) A review of the application of carbon materials in solar thermal energy storage. *Sol Energ* **192**, 35–68.
20. Chen MJ, He YR, Zhu JQ, Wen DS (2016) Investigating the collector efficiency of silver nanofluids based direct absorption solar collectors. *Appl Energ* **181**, 65–74.
21. Qu J, Zhang RM, Wang ZH, Wang Q (2019) Photo-thermal conversion properties of hybrid CuO-MWCNT/H_2O nanofluids for direct solar thermal energy harvest. *Appl Therm Eng* **147**, 390–398.
22. Nagata H, Hirano K, Miyako E, Nagata H, Hirano K, Hirotsu T (2008) Carbon nanotube-polymer composite for light-driven microthermal control. *Angew Chem Int Ed* **47**, 3610–3613.
23. Singh P, Campidelli S, Giordani S, Bonifazi D, Bianco A, Prato M (2009) Organic functionalisation and characterisation of single-walled carbon nanotubes. *Chem Soc Rev* **38**, 2214–2230.
24. Ghosh S, Dutta S, Gomes E, Carroll DD, Agostino R, Olson J, Guthold M, Gmeiner WH (2009) Increased heating efficiency and selective thermal ablation of malignant tissue with DNA-encased multiwalled carbon nanotubes. *ACS Nano* **3**, 2667–2673.
25. Miyako E, Itoh T, Nara Y, Hirotsu T (2009) Ionic liquids on photoinduced nanotube composite arrays as a reaction medium. *Chem A Eur J* **15**, 7520–7525.
26. Pastine SJ, Okawa D, Zettl A, Frechet JMJ (2009) Chemicals on demand with phototriggerable microcapsules. *J Am Chem Soc* **131**, 13586–13587.
27. Fujigaya T, Morimoto T, Niidome Y, Nakashima N (2008) NIR laser-driven reversible volume phase transition of single-walled carbon nanotube/Poly(N-isopropylacrylamide) composite gels. *Adv Mater* **20**, 3610–3614.
28. Barone PW, Baik S, Heller DA, Strano MS (2005) Near-infrared optical sensors based on single-walled carbon nanotubes. *Nat Mater* **4**, 86–92.
29. Hou PX, Liu C, Tong Y, Xu ST, Liu M, Cheng HM (2001) Purification of single-walled carbon nanotubes synthesized by the hydrogen arc-discharge method. *J Mater Res* **16**, 2526–2529.
30. Datsyuk V, Kalyva M, Papagelis K, Parthenios J, Tasis D, Siokou A, Kallitsis I, Galiotis C (2008) Chemical oxidation of multiwalled carbon nanotubes. *Carbon* **46**, 833–840.
31. Saini RK, Chiang IW, Peng H, Smalley SE, Billups WE, Hauge RH, Margrave JL (2003) Covalent sidewall functionalization of single wall carbon nanotubes. *J Am Chem Soc* **125**, 3617–3621.
32. Shen XN, Ji MZ, Zhang SM, Qin YJ, Zhang P, Wang YP, Guo Z-X, Pan MW, et al (2019) Fabrication of multi-walled carbon-nanotube-grafted polyvinyl-chloride composites with high solar-thermal-conversion performance. *Compos Sci Technol* **170**, 77–84.
33. Ornatska M, Peleshanko S, Genson KL, Rybak B, Bergman KN, Tsukruk VV (2004) Assembling of amphiphilic highly branched molecules in supramolecular nanofibers. *J Am Chem Soc* **126**, 9675–9684.
34. Miyagawa H, Misra M, Mohanty AK (2005) Mechanical properties of carbon nanotubes and their polymer nanocomposites. *J Nanosci Nanotechno* **5**, 1593–1615.
35. Tjong SC (2006) Structural and mechanical properties of polymer nanocomposites. *Mater Sci Eng R* **53**, 73–197.
36. Ajayan PM (1999) Nanotubes from carbon. *Chem Rev* **99**, 1787–1800.
37. Yang B-X, Shi J-H, Pramoda K, Goh SH (2008) Enhancement of the mechanical properties of polypropylene using polypropylene-grafted multi-walled carbon nanotubes. *Compos Sci Technol* **68**, 2490–2497.
38. Shi J-H, Yang B-X, Pramoda K, Goh SH (2007) Enhancement of the mechanical performance of poly (vinyl chloride) using poly (n-butyl methacrylate)-grafted multi-walled carbon nanotubes. *Nanotechnology* **18**, ID 375704.
39. Coleman JN, Khan U, Blau WJ, Gun'ko YK (2006) Small but strong: A review of the mechanical properties of carbon nanotube-polymer composites. *Carbon* **44**, 1624–1652.
40. Blake R, Coleman JN, Byrne MT, McCarthy JE, Perova TS, Blau WJ, Fonseca A, Nagy JB, et al (2006) Reinforcement of poly(vinyl chloride) and polystyrene using chlorinated polypropylene grafted carbon nanotubes. *J Mater Chem* **16**, 4206–4213.
41. Lourie O, Wagner HD (1998) Transmission electron microscopy observations of fracture of single-wall carbon nanotubes under axial tension. *Appl Phys Lett* **73**, 3527–3529.
42. Mizuno K, Ishii J, Kishida H, Hayamizu Y, Yasuda S, Futaba DN, Yumura M, Hata K (2009) A black body absorber from vertically aligned single-walled carbon nanotubes. *Proc Natl Acad Sci* **106**, 6044–6047.